Photoluminescence Characteristics of Y_2O_3:Eu^{3+} Nanophosphors Prepared Using Sol−Gel Thermolysis

J. Dhanaraj,[†] R. Jagannathan,*[,†,‡] T. R. N. Kutty,[§] and Chung-Hsin Lu[‡]

Luminescence Group, CECRI, Karaikudi 630006 (T.N), India, Materials Research Center, I.I.Sc, Banaglore 560012, India, and Department of Chemical Engineering, National Taiwan University, Taipei 106 Taiwan, R.O.C.

Received: May 21, 2001; In Final Form: August 5, 2001

Red emitting cubic Y_2O_3:Eu^{3+} nanophosphor with an average particle size in the range of 10−20 nm was synthesized using a more facile gel−polymer pyrolysis process. The maximum relative luminescence yield obtained for the nanophosphor prepared with a urea and PVA combination is about 30% in relation to the bulk Y_2O_3:Eu^{3+} industrial red phosphor. The photoluminescence excitation spectrum monitoring the dominant hypersensitive $^5D_0 \rightarrow {}^7F_2$ red emission of Eu^{3+} comprises two parts, viz., the dominant $Eu^{3+}-O^2$ charge-transfer band and a weak excitonic band (or its tail) corresponding to the $Y^{3+}-O^{2-}$ host matrix absorption. The relative strengths of these two bands have a strong dependence on the particle size. Furthermore, in this nanocrystalline insulator system having a band gap of about 6 eV, it is possible to observe a size dependent blue shift ($\sim$600 cm^{-1}) in the photoluminescence excitation band corresponding to the Urbach tail region of the yttria host matrix. Both the bulk and nanocrystalline Y_2O_3:Eu^{3+} show storage luminescence, a phenomenon previously unknown in this system. The mechanisms responsible for this appear to be different in these systems. The storage luminescence in the bulk system can be attributed to lattice defects, whereas that in the nanocrystalline counterpart is from a meta-stable, photoinduced surface-states arising from chemisorbed species.

1. Introduction

Nanophotonics, having made an impact in creating new technologies such as quantum well lasers and UV radiation blockers,[1] constitutes an important branch of optical materials. In particular, the doped nanocrystals, apart from their tremendous potential for applications, have emerged as an exciting field of materials research from the basic science point of view, because, in the nanocrystalline (nc) system, it is possible to acquire more reliable information on the spatially confined host−guest interactions, localized photo- and physicochemical reactions in the molecular level unlike the macroscopic systems where these are lost owing to ensemble averaging effects. For the preparation of nc ceramic systems, over the past decade, a number of new chemical techniques such as spray-drying, freeze-drying, sol−gel, coprecipitation, and self-sustaining combustion syntheses have been developed.[2−4] In general, currently known methods for nanocrystal synthesis that usually require a high degree of sophistication and control in various preparative parameters such as temperature or atmosphere or laser power etc., these pose serious limitations in scaling-up the synthesis for applications. In this investigation, we are reporting on a method quite suitable for the large scale synthesis of cubic Y_2O_3:Eu^{3+} nanocrystals whose bulk counterpart is an efficient red luminophor extensively applied in the lighting industry[5] and plasma display panels (PDP).[6] The nc analogues of these ceramic systems seem to hold some promise for future applications such as display materials with low energy excitation sources.[7]

Self-propagating high temperature synthesis of phosphor materials is widely acknowledged as a method for the synthesis of micron sized particles.[8] This method has the drawback of producing highly agglomerated particles. When this method is used along with a polymer, it is possible to produce well-dispersed nanoceramic materials. In this investigation, we have employed a polymer pyrolysis method using various organic polymers. The organic polymer(s) employed can serve both as a fuel for the nanocrystal formation and as a dispersing medium, limiting the agglomeration of particles. In this context, it should be mentioned that there are already reports using poly(vinyl alcohol) (PVA) and urea combinations for the synthesis of various nanoceramic materials.[9] However, the trials with poly(acryl amide) (PAM) for the preparation of various nanoceramics have gained importance only recently.[10]

The salient features of this facile synthesis are inexpensive precursors, the scope for large scale synthesis, and high relative luminescence yield. We believe that this method may provide wider scope for tailorability, precise control on the particle- size, and morphology for Y_2O_3:Eu^{3+} nanocrystals. It should be mentioned that Y_2O_3:Eu^{3+} nanocrystals prepared using this method adopt a cubic structure, whereas all other reports except by one group[11] were on monoclinic Y_2O_3:Eu^{3+} nanocrystals[12−14] showing several anomalous fluorescence properties which render them unfavorable for lighting applications.

Furthermore, we have found that under excessive UV excitation, both the bulk and the nc counterparts show a new phenomenon similar to storage luminescence. Although the bulk Y_2O_3:Eu^{3+} phosphor has been applied in industry for the past three decades, surprisingly, there are no reports on the optical storage property observable in this system. The storage luminescence property observable in the Y_2O_3:Eu^{3+} system appears to originate from a sort of recuperation of photogenerated

* To whom correspondence should be addressed. E-mail: jags57_99@yahoo.com.
[†] Luminescence Group, CECRI.
[‡] National Taiwan University.
[§] Materials Research Center, I.I.Sc.

10.1021/jp0119330 CCC: $20.00
Published on Web 10/12/2001

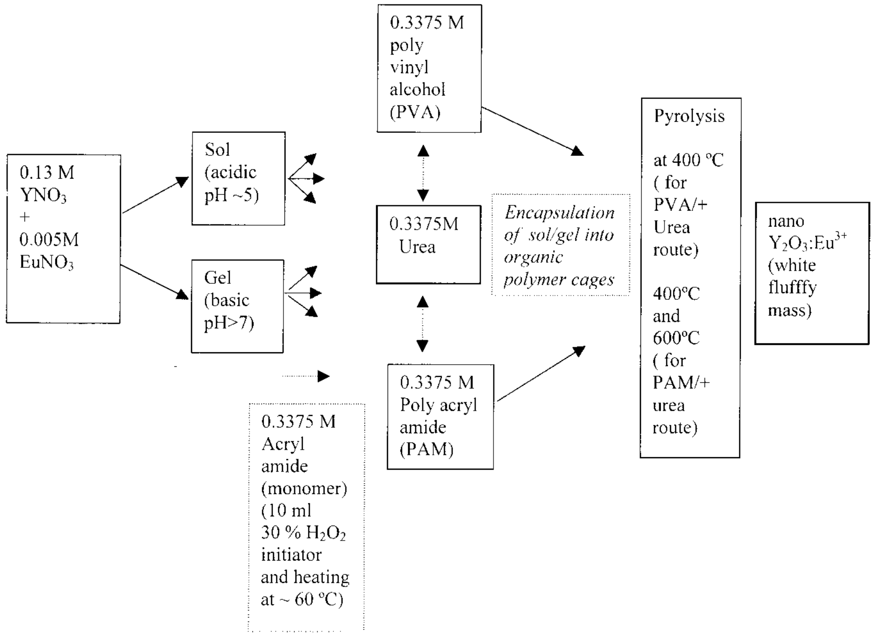

Figure 1. Flowchart illustrating the preparation of $Y_2O_3:Eu^{3+}$ nanophosphor by sol−gel pyrolysis. The double sided arrows indicate that the samples are prepared with or without the addition of urea.

TABLE 1: Least Squares Refined (Space Group *Ia*3) Unit Cell Parameters for Differently Prepared $Y_2O_3:Eu^{3+}$ Nanocrystalline Samples

system (sample)	*a* (Å)	std. error for a_0 (Å)	cell volume (Å)^3	% of deviation in cell volume from the std
JCPDS std no. 43-1036	10.604		1192.4	
bulk-standard[a]	10.579	± 0.008	1183.8	± 0.72
b	10.574	± 0.009	1182.1	± 0.86
c	10.582	± 0.01	1185.1	± 0.61
d	10.547	± 0.016	1173.2	± 1.61
e	10.559	± 0.013	1177.2	± 1.27
f		data could not be refined		

[a] Bulk standard. [b] $YEu(NO_3)_3$ sol + urea + PAM. [c] $YEu(NO_3)_3$ gel + urea + PAM. [d] $YEu(NO_3)_3$ sol + PAM. [e] $YEu(NO_3)_3$ sol + urea + PVA. [f] $YEu(NO_3)_3$ sol + PVA.

carriers. This is found to be critical in sample preparation conditions, especially in the atmosphere/partial oxygen pressure used in the phosphor preparation. Although this phenomenon is observable in both the bulk and nc systems there seems to be several differences including the origin of this phenomenon. Furthermore, we observed a blue shift of about 600 cm^{-1} (∼0.08 eV) in the Urbach tail region corresponding to the fundamental absorption edge of the insulating nc Y_2O_3 host system. This manifests in the satellite excitation band in the higher energy side of the spectra feeding various localized f−f levels of Eu^{3+} through excitonic transitions. We organized this paper into two parts focusing on (i) the nanocrystal synthesis and its characterization and (ii) the luminescence processes involved, including a detailed discussion on the possible origin of the storage luminescence observed.

2. Experimental Section

2.1. Nanocrystal Synthesis. The details of $Y_2O_3:Eu^{3+}$ nanocrystal synthesis by sol−gel thermolysis is schematically illustrated in Figure 1, and the details of chemical compositions for various samples are given in Table 1. In this work, we employed urea as the fuel to produce high temperature and/or PAM/PVA as the dispersing agent. It appears that the organic polymers apart from serving as dispersing media can serve as a secondary fuel because of the presence of amide or alcohol groups producing a strong exothermic reaction. Stoichiometric compositions of the redox mixture for the combustion reaction were calculated using the total oxidizing (O) and reducing (F) valencies of the components that serve as the numerical coefficients for the stoichiometric balance so that the equivalence ratio (ϕ_e) was maintained at unity (O/F = 1) so that the energy released by the combustion is maximum.[4] For urea as the fuel, the valency was calculated to 6^+, and for $Y(NO_3)_3$ it was calculated to 15^-. Thus, the stoichiometry for the preparation of Y_2O_3 (+ Eu_2O_3) from $Y(NO_3)_3$:urea was 1:2.5. The amount of PVA or PAM was optimized empirically. The formation of Y_2O_3 crystallites from the starting materials (for the PVA system as an example) follows the eq 1:

$$(2\text{-}x)Y(NO_3)_3 + x\,Eu(NO_3)_3 + 5\,NH_2\text{–}CO\text{–}NH_2 + 5(CH_2\text{-}\underset{\displaystyle CH_2\text{-}OH}{\underset{|}{CH}})_n \rightarrow$$
$$Y_{2-x}Eu_xO_3 + (5+n)\,CO_2 + 5NH_3 + 5NO_2 + (5+n)H_2O \text{ -----} \qquad (1)$$

Mixed $(Y/Eu)(NO_3)_3$ stock solution was prepared using 0.13 M YNO_3 and 0.005 M $EuNO_3$ solutions obtained from the corresponding oxides (of 99.9% purity as obtained from Indian Rare Earths) by dissolving in dilute nitric acid (analyzed reagent). To this solution, 0.3375 M urea and 0.3375 M acrylamide monomer (or 0.3375 M PVA) solution were added, and the solution was thoroughly stirred. This mixture was polymerized by adding 10 mL of 30% H_2O_2 initiator and heated to 60 °C in order to accelerate the polymerization process. The total reaction volume was 50 mL. The concentration of Eu^{3+} was fixed at an optimum value of 4% (wrt Y^{3+}) in all cases. For the sol−gel preparation, 1% ammonia solution was added to 10 mL of the stock solution in a beaker at the rate of 10 drops per min to precipitate $Y/Eu(OH)(CO_3)$ gel. Adding an initiator along with urea polymerized the solution. The excess water was evaporated at 100 °C. The resulting precursor polymer gel was treated as above.

The precursor (either the sol or the gel) thus prepared was pyrolyzed at 400 °C for about 30 min. The product obtained on combustion of this mixture produced a highly fluffy,

voluminous carbonaceous mass. This product was not ground, as otherwise the grinding produces coarse, sintered particles during further heat treatment for the removal of carbon. Hence, the as prepared carbonaceous mass was heated around 600 °C for about 2 h (in some cases between 400 and 600 °C) so that the carbon was removed completely and produced fine grains of nanosized Y_2O_3:Eu particles. It is important to mention that the presence of carbon network/cages can completely prevent particle agglomeration even when heat treated at high temperatures around 600 °C. When PVA was used, the resulting precursor did not pass through the carbonaceous phase as the PVA decomposed along with the urea at much lower temperatures (∼400 °C). The samples were not further surface treated, and all of the measurements were made within a few hours (1−3 h) of sample preparation.

2.2. Characterization. To compare the fluorescent properties of the nanophosphors with that of the bulk system, we prepared the corresponding $Y_{2-x}O_3$:Eu_x^{3+} bulk phosphor system (with $x = 4\%$) using solid-state reaction methods at 1200 °C for 4 h in an ordinary lab atmosphere.[15] For comparison, we used a commercially available Y_2O_3:Eu^{3+} red phosphor sample manufactured by the Nichia Company, Japan. Both of these bulk samples had an average particle size of 5 μm as measured using a laser based Malvern particle size analyzer.

The chemical purity of these products was checked by X-ray powder diffraction (XRD) patterns at room temperature using JEOL 8030 powder diffraction system with Cu Kα radiation. The photoluminescence measurements were made using a Hitachi 650-10S fluorescence spectrophotometer employing Hamamatsu R928F photomulitplier as the light detector, gratings with a groove density of 600 lines/mm and a 150 W Xe arc discharge lamp as the excitation light source. The excitation spectra were corrected for the beam intensity variation in the Xe light-source used. STA 1500 PL from Thermal Sciences, U.K. differential thermal analysis system was employed to follow the thermolysis process during the nanocrystal synthesis. The various exothermic peaks and the corresponding thermogravimetry analyses correlated well with one another, and the detailed results of the thermal analysis and other material synthesis aspects will be published separately. To analyze the reaction product for a possible chemisorbed gases or moisture we measured infra- red spectra for these samples using a Perkin-Elmer model Paragon-500 FTIR spectrophotometer (in dry KBr mounts). The yttrium (Y^{3+}) content in various samples was analyzed (in relation to Y_2O_3 starting material with 99.99% purity as obtained from Indian Rare Earths as the reference) using a CMI XRX-XYZ series X-ray fluorescence spectrophotometer (XRF). For UV exposure (for the storage luminescence) and curing (for the FTIR studies), we used the Xe lamp of the fluorescence spectrophotometer tuned for 260 nm with a slit width of 20 nm corresponding to a power level of 3.5 W/cm^2 or a 20 W mercury discharge lamp along with a UV filter having band-pass maximum at 254 nm, respectively. The duration of UV exposure/curing varied between 5 and 10 min to 2 h as indicated in the respective sections. The morphology and the particle size of the nanoceramic material synthesized were analyzed using a JEOL 200 CX transmission electron microscope (TEM) operated at 200 kV. Thermally stimulated luminescence glow curves for the UV exposed samples were recorded by following the same procedure as described earlier.[16]

3. Results and Discussion

3.1. Nanoparticle Growth−X-ray Diffraction and Electron Microscopy Studies. All of the samples (both the nano and the bulk samples) obtained were phase pure, and the diffraction patterns obtained (Figure 2) are well indexable under cubic bixbyite type matrix having *Ia3* lattice symmetry. The least squares refined crystallographic unit cell parameter values obtained for all of the samples are in good agreement with the standard values given in JCPDS # 43-1036 (Tabe 1).

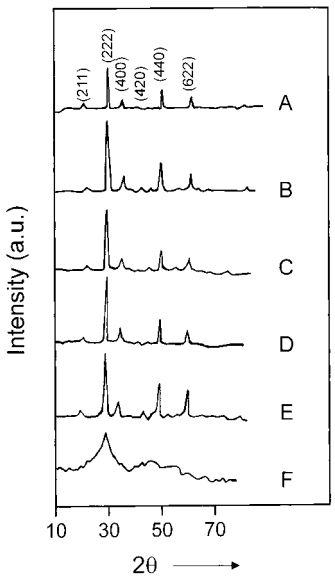

Figure 2. X-ray diffraction pattern (using Cu Kα at $T = 300$ K) for various samples compared with the bulk standard sample (A). The compositions for the preparation for the nanocrystalline samples: (B) $YEu(NO_3)_3$ sol + urea + PAM; (C) $YEu(NO_3)_3$ gel + urea + PAM; (D) $YEu(NO_3)_3$ sol + PAM; (E) $YEu(NO_3)_3$ sol + urea + PVA; (F) $YEu(NO_3)_3$ sol + PVA.

The TEM pictures (Figure 3) for the samples B and E prepared respectively with $(YEu)NO_3$ sol + urea + PAM and $(YEu)NO_3$ sol + urea + PVA based systems clearly show that the particles are well dispersed crystallites. The nanoparticles with polyhedral morphology have a size distribution in the range of 10−20 nms. Furthermore, from the TEM figure we can observe a regular hexa-net feature for the polyhedral particles. Hence, we believe that the residual carbon network resulting in thermolysis may provide the basic structural framework for the crystallite growth. For the $(YEu)NO_3$ sol along with either PAM- or PVA-only systems (samples D and F without any urea), the resulting sample on pyrolysis yielded highly agglomerated particles embedded on a film like structure without any distinct morphological features. It is reasonable that, in the former case, the combined fuel system because of PAM/PVA and urea accelerated the crystallization process owing to the generation of very high in situ temperatures. This will give a better scope for the particle growth yielding well-dispersed larger particles. The latter can be explained in terms of the lack of sustained combustion reaction probably due to the low calorific value of the PVA/PAM. Intriguingly, the gel based preparations (sample C) again yielded highly agglomerated particles with no clear morphological features. We consider any detailed discussion concerning the agglomerated particles beyond the scope of this investigation.

The interplanar spacings calculated from selected area electron diffraction (SAED) patterns for samples B and E (given as insets in the respective figures) are consistent with the corresponding values given in the standard JCPDS file. It was found that, for these samples employing either urea and PAM or urea and PVA combinations, the SAED patterns had spotty annular rings clearly verifying the polycrystalline nature of the samples. For the other samples, the SAED patterns were highly diffused

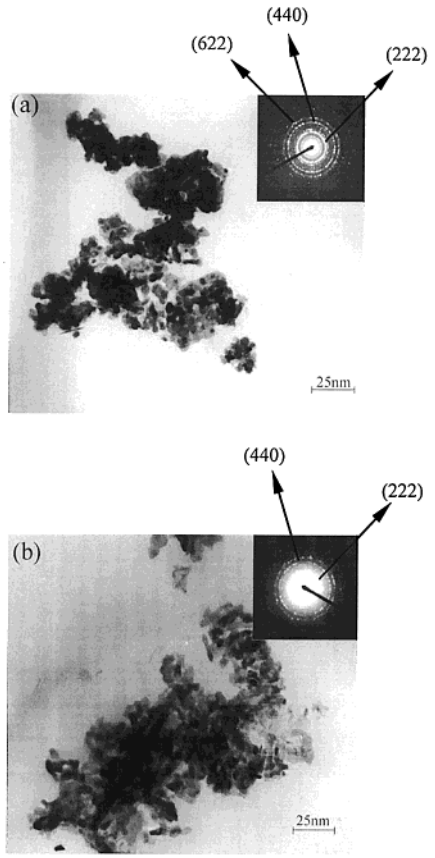

Figure 3. Transmission electron microscopy images of nanocrystalline Y_2O_3:Eu^{3+} (a) sample B $YEu(NO_3)_3$ sol + urea + PAM system and (b) sample E $YEu(NO_3)_3$ sol + urea + PVA system. The inset shows the corresponding selected area diffraction (SAED) patterns of the respective samples. The interplanar spacings are consistent with the standard JCPDS file no. 43-1036.

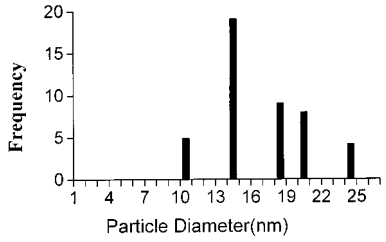

Figure 4. Histogram showing the particle size distribution, experimentally counted for sample B prepared with the $YEu(NO_3)_3$ sol + urea + PAM system.

spotty rings, which make further insight on these samples difficult. The histogram depicted in Figure 4 gives the particle size distribution of the experimentally counted particles corresponding to sample B prepared with $YEu(NO_3)_3$ sol + PAM + urea, and as can be seen, the average particle size is around 14 ± 1 nm. For comparison, we measured the particle size for some of these samples from the XRD line-width data applied in the Scherrer equation.[17] From the XRD line-width data for the most intense (222) line at 2 Å =29.4°, as representative examples, the particle sizes of the sample B (with $YEu(NO_3)_3$ sol + urea + PAM) and sample D (with $YEu(NO_3)_3$ sol + PAM.) were found to be respectively 12 and 10 nm. These results support our observation through TEM that the combined fuel system (urea + PAM) produced larger nanoparticles.

3.2. Photoluminescence Processes. *3.2.1. Charge Transfer and Exciton Assisted Luminescence Processes.* On UV excitation (λ_{exc}= 250−260 nm), both the bulk and all of the nc

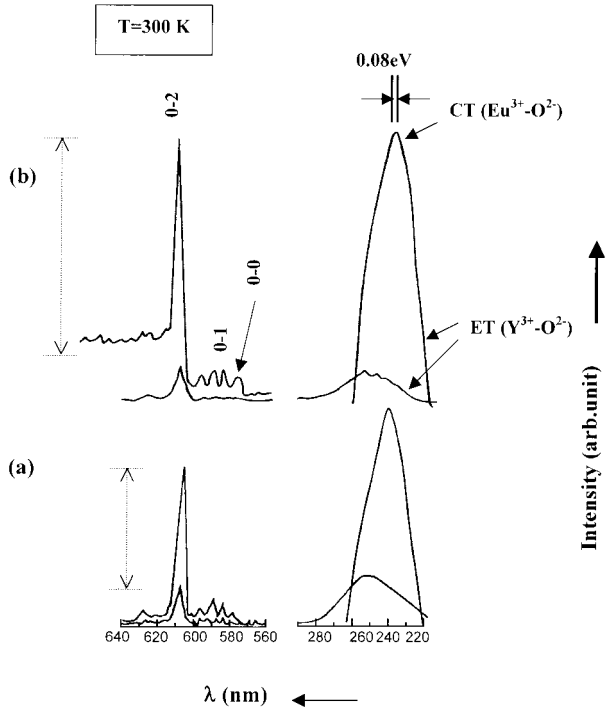

Figure 5. Photoluminescence emission and excitation spectra of (a) Y_2O_3:Eu^{3+} bulk and (b) Y_2O_3:Eu^{3+} nanocrystalline sample B prepared with $YEu(NO_3)_3$ sol + urea + PAM. Eu^{3+} concentration was 4% in both cases. The experimental conditions for the spectral recordings were the same in both cases. The positions of the various photoluminescence (PL) transitions seen as sharp lines marked 0−0, 0−1, and 0−2 are the same in both cases and correspond to $^5D_0 \rightarrow {}^7F_J$ transitions from Eu^{3+}. The double sided arrows indicate the enhancement in photoluminescence emission intensity corresponding to the $^5D_0 \rightarrow {}^7F_2$ transition of Eu^{3+} under excessive photoexcitation at 260 nm, 3.5W/cm^2 for 10 min. The spectra were recorded immediately (within 1 min) after the excessive photoexcitation and the spectral measurement conditions (slit width and scan speed) were the same both before and after photoexcitation. The blue shift by 0.08 eV in the excitonic excitation band for the nanocrystalline sample is indicated.

Y_2O_3:Eu^{3+} samples yield intense red emissions around 610 nm (Figure 5). The red emission comes from Eu^{3+} center(s) (having $4f^6$ electron configuration) can be assigned to the hypersensitive $^5D_0 \rightarrow {}^7F_2$ transition working using a forced electric dipole transition mechanism. This is a parity forbidden *f*−*f* intraconfigurational transition. In the cubic bixbyite type Y_2O_3, there are two types of cationic sites occupied by Y^{3+} (hence Eu^{3+}) having either C_2 and S_6 local symmetries. The former site lacking inversion center is quite favorable for observing the electric dipole transition as a forced transition due to the admixture of the odd parity states, whereas the latter is unfavorable for the electric dipole transition due to the presence of the inversion center. The minor emission components in the orange region around 590 nm due to the $^5D_0 \rightarrow {}^7F_1$ magnetic dipole transition are structurally independent. For this reason, this transition can be used as an internal standard[18] to gain some idea of the relative transition strengths of the other transitions of Eu^{3+}. Because of the limited spectral resolution in our experimental setup, it was not possible for us to gain more information on the possible multiple sites occupied by Eu^{3+} in the nc system. Notwithstanding this limitation however, from the fluorescence spectra, it is obvious that the Stark splitting pattern observed in the various Eu^{3+} levels are the same both in the nano and bulk systems. This suggests that the local symmetries in both the bulk and the nc are the same. Further, the excitation spectrum (Figure 5) monitoring the red emission

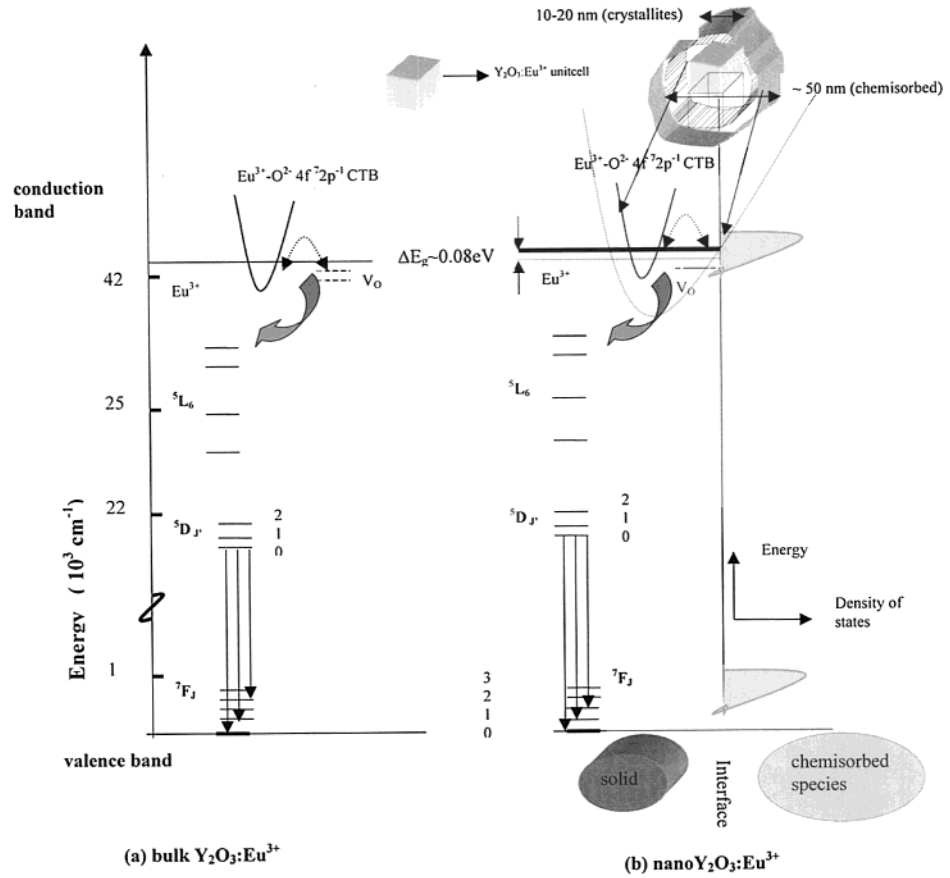

Figure 6. Energy level diagram with schematic illustration of the photoluminescence processes between the Y_2O_3:Eu^{3+} bulk and nanocrystalline samples. V_o represents the position of oxygen vacancies. ΔE_g denotes the blue shift observed in the excitation band corresponding to exctionic transitions in the nanocrystalline system.

(due to the hypersensitive $^5D_0 \rightarrow {}^7F_2$ transition of Eu^{3+}) shows an asymmetric band (skewed toward higher energy side) with the maximum around 250 nm (~4.96 eV). This corresponds to the Eu^{3+}-ligand electron-transfer transition ($4f^7 2p^{-1}$ charge-transfer band *CT*) lying in the band gap region of the Y_2O_3 host matrix.[19]

The asymmetric excitation band implies the superimposition of an additional excitation component on the higher energy side of the excitation band. It is well-known that the fundamental absorption edge of the yttria matrix sets in around 200 nm (much below the range of our fluorescence spectrophotometer). Also it has been reported that the absorption tail- the Urbach tail extends up to 5.2 eV (240 nm) and shows an excitonic peak (ET) around 230 nm (5.3−5.5 eV) due to $O^{2-} \rightarrow Y^{3+}$ ($2p^{-6} \rightarrow$ 5s) electron transfer (CT) transition.[20,21] The presence of electron holes in the p state of oxygen lying in close proximity with the Y^{3+} site may result in excitons. Upon UV excitation, these two processes will compete with one another. The absorption coefficient of the excitonic process is much stronger ($\alpha = 10^5$ cm^{-1}) than the CT process, as the latter involves an absorption in the sub-bandgap region of the host matrix. However, with the excitonic process being a surface property, it is strongly quenched at the innumerable recombination sites at the surface of the crystallite (especially when the penetration depth of the excitation is limited to about 100 nm), and hence, the CT process will dominate.[22] This can explain the intense charge-transfer excitation band feeding energy to the various localized *f*−*f* levels of Eu^{3+} in the subband gap region, in particular the $^5D_0 \rightarrow {}^7F_J$ manifold as illustrated in Figure 6. It is certainly intriguing that for the UV exposed sample the ET band gains considerable intensity over the CT band (Figure 5, and Table 2). Although this phenomenon is observable both in the bulk and nc system, this effect seems to be more prominent in the nc counterpart attributed to the presence of innumerable surface states in the latter.

TABLE 2: Comparison of Photoluminescent Properties of Bulk and Y_2O_3:Eu^{3+} Nanocrystals

sample	TEM particle size (nm)	%Y^{3+} wrt pureY_2O_3	relative lumin. yield	relative intensity of $^5D_0 \rightarrow {}^7F_2/{}^5D_0 \rightarrow {}^7F_1$ before UV exposure	relative intensity of $^5D_0 \rightarrow {}^7F_2/{}^5D_0 \rightarrow {}^7F_1$ after UV exposure	ET/CT ratio after UV exposure
a	~5μ*	93.2	100	2.6	11.9	3.9
b	14 ± 1	90.4	33	10.0	13.4	10.4
c	*f*	91.3	16			
d	*f*	90.9	18			
e	16 ± 1	91.2	37			

[a] Bulk (*standard value). [b] $YEu(NO_3)_3$ sol + urea + PAM. [c] $YEu(NO_3)_3$ gel + urea + PAM. [d] $YEu(NO_3)_3$ sol + PAM. [e] $YEu(NO_3)_3$ sol + urea + PVA. [f] Agglomerated particles.

3.2.2. Blue Shift the Urbach Tail in Y_2O_3 Due To Size Effect. Recently it has been shown that the cubic Y_2O_3:Eu^{3+} nc sample prepared using a chemical vapor reaction method (of size 10 nm) shows a blue shift in the host absorption and excitation bands (corresponding to the excitonic process), whereas no such effect is observable in the $Eu^{3+}-O^{2-}$ charge-transfer band.[22] The Urbach tail in the Y_2O_3 matrix (for a single crystal of size 3 mmϕ × 8 mm) due to the O^{2-} (valence band) to Y^{3+} (conduction band) excitonic transition sets in around 5.2.eV at room temperature.[20] This is expected to shift toward higher energy as the crystallite size is reduced as can be explained by the Urbach relation. Recently, Konrad et al.[11] demonstrated such a quantum size shift toward higher energy by 5 nm in the

excitation band corresponding to excitonic transition for the Y_2O_3:Eu^{3+} nc system with respect to that of the bulk sample. Further, Schmechel et al.[22] reported recently a size dependent blue shift in the excitonic band. Apart from this observation, they demonstrated that the charge-transfer excitation band (having no size dependence) has a profound dependence upon the chemical surroundings of the host matrix. Our results are in good agreement with these reports. We also observed a similar blue shift in the excitonic band by about 600 cm^{-1} (0.08 eV) notwithstanding the fact that we followed a different chemical route for the preparation of Y_2O_3:Eu^{3+} nc sample. It is really amazing that such a quantum size effect is observable even in this insulator system with a band gap of about 6 eV.

3.2.3. Defects and Chemisorbed Species as Possible Precursors for Exciton States and Storage Luminescence. It is rather surprising that there are no reports on the optical storage luminescence exhibited by this important industrial phosphor being used in the lighting industry for three decades. All of the bulk samples (both commercial and the lab prepared samples) showed this intense storage luminescence property. For the bulk samples obtained from different sources, there was a difference in the relative intensity of the storage luminescence and the storage property with respect to time. These differences may be due to different heat treatment conditions adopted (in particular the partial pressure of oxygen) by the phosphor manufacturers. Aliovalent substitution such as alkaline earth(s) impurities in theY^{3+} sites (Ca^{2+}, Sr^{2+}, etc.) and the use of fluxes (such as NaCl, NaF, etc.) in the phosphor synthesis drastically reduce the oxygen vacancies in the yttria matrix.[15,23] This can in turn lead to a significant reduction in the nonradiative losses of the excited energy in the higher excited states via the oxygen vacancies paving way for the enhanced luminescence yield. Obviously, the commercial samples yielded higher luminescence yield with the quantum yield nearing unity.[24] In any case, the storage luminescence is an undesirable property for a lighting phosphor, as this implies a decrease in the luminescent yield. This clearly fixes oxygen vacancies or other bulk defects as the cause for the storage luminescence in the bulk Y_2O_3:Eu^{3+} system.

For the nc analogue, this phenomenon was observable only in the case of Y_2O_3:Eu^{3+} nanocrystals prepared using PAM and urea + PAM combinations, whereas there was no measurable storage luminescence in the case of nc samples prepared with PVA and urea + PVA combinations. Hence, we compare and present the results of storage luminescence between the bulk sample and the nanocrystals prepared using PAM and urea combination only (Figure 5). We observed that the storage luminescence property undergoes faster fading in the bulk sample (lasting for about 50−60 s) when compared to that in the nc system where this lasts longer (for about 20 min).

The following points are pertinent to explain the difference observed between the bulk and nc systems:

From the XRF studies, it has been found that the Y^{3+} content was about 2% less in the nc system when compared with that in the bulk system (Table 2). This implies a significant increase in the lattice vacancies (due to Y^{3+} sites). Further, we observed that for the UV exposed bulk sample (at 260 mm for 10 min with a power level of 3.5 W/cm^2) there was a 4-fold increase in the relative intensity of the hypersensitive $^5D_0 \rightarrow {}^7F_2$ emission with respect to $^5D_0 \rightarrow {}^7F_1$ transition, whereas there was only 30% enhancement in the same ratio for the nc system. The ratio between intensities of ET to CT bands was much higher (about 10) for the UV exposed nc system, whereas the same ratio was only 4 for the bulk system. We observed that the thermally

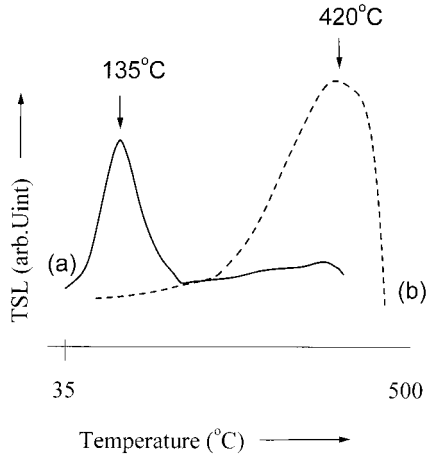

Figure 7. Thermally stimulated luminescence (TSL) glow curves for (a) bulk Y_2O_3:Eu^{3+} and (b) nanocrystalline sample B prepared with $YEu(NO_3)_3$ sol + urea + PAM. The spectra were recorded after exposing both samples to the same level of UV dose as given in Figure 5. Both samples had the same Eu^{3+} concentration of 4%.

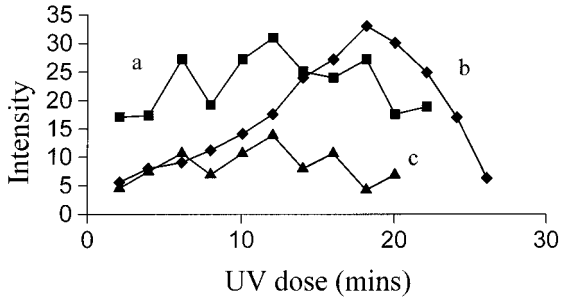

Figure 8. Variation in storage luminescence intensity (for the $^5D_0 \rightarrow {}^7F_2$ red emission of Eu^{3+}) versus UV dose in terms of exposure time (with the same UV power as given in Figure 5). The error in the storage luminescence intensity values (in arb. units) was about ±1%, sample A bulk system; (b) nanocrystalline sample B prepared with $YEu(NO_3)_3$ sol + urea + PAM system and (c) sample B after vacuum treatment (at 10^{-5} mm of Hg for 1 h).

stimulated luminescence (TSL) glow curves for the UV irradiated bulk and nanocrystals were considerably different. From Figure 7, we can see that the bulk sample has shown the TSL maximum at 135 °C corresponding to a shallow level, whereas the nc sample B has shown a peak at 420 °C suggesting a deeper trap level. These results suggest different types of defect complexes involved in the bulk and nc systems.

More importantly, there is a remarkable difference in the UV dose versus storage luminescence patterns between the bulk and nc samples (Figure 8). The former exhibited a reproducible saw-tooth pattern, whereas the latter showed a simple Gaussian type pattern. Curiously, once the nc sample (sample B) was treated under high vacuum (at 10^{-5} mm of mercury) to remove any possible extraneous chemisorbed species, the UV dose versus storage luminescence response showed a pattern similar to that of the bulk sample. Furthermore, the vacuum-treated nc sample did not show any storage luminescence effect. These observations make us to hypothesize that the origin of the storage luminescence in the nc sample can be related to some kind of chemisorbed species.

The innumerable surface states present in the nc system can have considerable influence on the optical properties. The different possibilities are (i) the defect states, cation/anion vacancies, and interstitials ($V_Y/V_O/O_I$) with energy levels located within the band gap and (ii) surface states (SS) related to the adsorbed species or surface defects where energy levels are

within the band gap; these will be labile with pressure or size factor conditions.

The storage luminescence and the related processes due to crystalline lattice vacancies will be considerably different from that of the chemisorbed species. The former can prevail in bulk system as well and this will be determined by the Y(+Eu) to O ratio. The adsorbed species can have energy states fluctuating with variable density of states. This is because that they are not an integral part of the solid but form extraneous gas (or liquid) phase related species. They do not have any fixed position in the energy level diagram, yet, are located within the band gap region. These are surface defects related, i.e., defects toward the solid side of the interface, yet they are not found in the bulk system arising from surface reaction(s). Owing to the pronounced surface-to-volume ratio of the nanocrystals, these levels acquire significance. However, because of the limitation of our present experimental setup, we are unable to pick up any specific information concerning the nature of the surface states and their possible symmetry configurations. However, we have schematically illustrated the above and also the possible effect of chemisorbed species on the Eu^{3+} luminescence processes in Figure 6.

The relative luminescence yield for the nc sample E prepared using ($YEuNO_3$) sol + urea + PVA system with an average particle size of 16 nm presented the highest value of about 37% with respect to the bulk phosphor (Table 2). However, the nc sample C prepared using ($YEuNO_3$) gel + PAM + urea system yielding highly agglomerated particles gave the lowest luminescent yield of 16%. It is important to note that the samples prepared from the gel-based precursor starting material produced highly agglomerated particles with no individual particle characteristics. However, for reasons of completeness, we present some of these results in Table 2 and we consider any further discussion on the gel-based system as beyond the scope of this investigation. Also, it should be noted that samples B and D corresponding to ($YEuNO_3$) sol + PAM with and without urea showed intense storage luminescence, with the relative luminescence yield respectively being 33 and 18%. On the other hand, Schmechel et al[22] reported a lower value of less than 10% for nanoparticles of size 10 nm prepared using chemical vapor reaction method (CVR).

We consider that such a large difference in the luminescence yield cannot be fully accounted for only based on size considerations. This is because the effect(s) of surface states predominantly serving as the recombination sites will act as luminescent quenchers and this cannot be overlooked.

The highly reactive nature of the porous nanoparticles will show a pronounced propensity to chemisorb gases that may evolve during the course of nanocrystal synthesis. On comparison of the FTIR spectra of nanoparticles prepared using ($YEuNO_3$) sol + PAM + urea system (sample B) and the bulk system (sample A) given in Figure 9, it is obvious that the nc sample shows intense absorption around 3500, 2750, and 1500 cm^{-1}. Although the absorption in these regions has ammonium/cyano−amine groups signature, the presence of the hydroxyl group due to contamination of the nano particles by moisture should also be considered. Furthermore, for the heat treated sample at 800 °C for 3 h, the intense absorptions around 3500 and 1500 cm^{-1} go down in intensity, whereas the absorption around 2750 cm^{-1} gains considerable intensity. We could not observe much difference in the absorption bands around 3500 and 1500 cm^{-1} between the freshly prepared and the UV-cured sample (using an UV lamp giving maximum emission at 254 nm and with a rated power of 20 W for 2 h). Interestingly, the

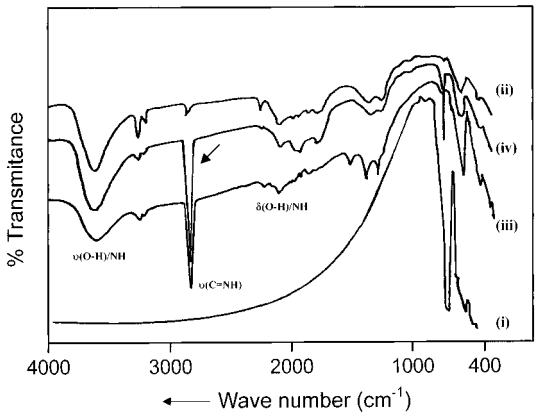

Figure 9. FTIR spectra of samples under different conditions (i) bulk $Y_2O_3:Eu^{3+}$; (ii) freshly prepared nanocrystalline $Y_2O_3:Eu^{3+}$ sample B; (iii) the sample as in (ii) heat treatment in air at 800 °C for 2 h; (iv) the sample as in (ii) after UV exposure 254 nm from 20 W UV lamp for 2 h. The solid arrow indicates the increase in the absorption at 2750 cm^{-1} after the UV exposure.

sharp absorption line around 2750 cm^{-1} gains considerable intensity both under UV curing and with heat treatment. The above results clearly lead us to conclude that the hydroxyl ion contamination (implied by ν(O−H) and δ(O−H) absorptions respectively around 3500 and1500 cm^{-1}) is a dominant process in the nc system investigated. Furthermore, the significant enhancement observed in the intensity of the sharp line absorption around 2750 cm^{-1} (that can reasonably be assigned to an ammonium/cyano-amine group) clearly suggests the presence of chemisorbed species undergoing considerable photochemical modification.

To explain the possible effects of these chemisorbed species, we have to first consider the multiphonon emission leading to luminescence quenching. The scope for the multiphonon relaxation through the vibration of the yttria matrix can be ignored because of the low-frequency involved by the host matrix (~600 cm^{-1}). On the other hand, the high-frequency vibration around 3500 cm^{-1} is very important to account for the low luminescence yield observed in the nc system. Because, in this case only, low numbers of phonons are required for the nonradiative luminescence quenching of the transition. Schmechel et al.[22] explained the low luminescence yield, a value as low as 3% in this system, in terms of high-frequency vibrations of the adsorbed hydroxyl species (OH^-). We consider that this cannot adequately explain our results that the nc samples undergo drastic changes in luminescence characteristics such as initial luminescence build up (storage type) and the subsequent drastic decrease in the luminescence yield due to some photo degradation process. Also, we believe most of these results can be explained on the basis of some kind of exciton annihilation process.

We also observed such a high-frequency component around 3500 cm^{-1} in the FTIR spectrum of the nc sample(s), but the relative luminescence yield is about one order higher than that reported by Schmechel et al.[22] This predicts a slightly lower value of about 200 s^{-1} for the nonradiative relaxation rate than that reported by Schmechel et al.[22] Now the pertinent logical question is, if multiphonon relaxation via chemisorbed hydroxyl ions has been the active mechanism how was it possible to realize such a high luminescence yield (of about 30%) in the samples investigated? This is too high a value to be bridged by nonradiative multiphonon relaxation with in the ^5D_J manifold. Alternatively, we consider it more plausible that a photostimulatable luminescence complex (induced by the presence of

chemisorbed species) sets in immediately after the UV exposure. This may modify the chemistry of the surface states, probably acting as precursors for exciton states (electron−holes in close proximity). The excitons thus created can play the role of energy carriers facilitating higher luminescence yield in the nc samples investigated. This process acquires significance for near band edge excitations. The relaxation geometry (the intersection geometry with the ^5D_J manifold of Eu^{3+} in the photoexcited state as indicated in Figure 6) and the kinetics of the metastable state due these surface state(s) may determine the luminescence yield (also the luminescence buildup and subsequent degradation on UV exposure) of the nc system.

It has been found that the luminescence yield and the storage luminescence have profound dependence on various polymers employed. This suggests that the configuration and the relaxation processes are determined by the nature of the chemisorbed species involved. Furthermore, the drastic difference observed in the time scales of storage luminescence between the bulk and nanocrystals confirms that the relaxation geometry for the luminescence center acquiring prominence upon excessive photoexcitation are different in both cases. In this context, it is pertinent to point out that recently studies reporting "quantum blinking/on−off" switching behavior in several nc semiconductor and insulators (including the Y_2O_3:Eu^{3+} system) having profound dependence on the excitation conditions.[25,26] This correlates well with our observation of storage luminescence and thus meriting further detailed studies in this direction on this important luminescent system.

4. Conclusions

The preparation of Y_2O_3:Eu^{3+} nanophosphors (of size 10−20 nm) using a gel−polymer pyrolysis appears to be a more feasible method for the large scale production. A typical preparation employing the [$YEu(NO_3)_3$] sol + PVA polymer + urea system yielded nanoparticles with 15 nm average size and produced a relative luminescence yield of about 35% with respect to the bulk red phosphor. This value was about one order higher than the value of luminescence yield reported for the nanophosphors prepared using other methods. The photoluminescence excitation monitoring red emission from Eu^{3+} occurs through two processes (apart from direct excitation in the *f*−*f* levels of Eu^{3+}), viz, Eu^{3+}−O^{2-} charge transfer and the exctionic Y^{3+}−O^{2-} electron-transfer mechanisms. For the nc system, the relative intensity between these two processes goes in favor of the latter because of the pronounced surface states acting as precursors for the excitons. A size dependent blue shift of about 600 cm^{-1} in the excitation band corresponding to the fundamental absorption edge of Y^{3+}−O^{2-} matrix system was also confirmed.

This system (both bulk and nc analogues) shows intense storage luminescence, a property so far not known in this system. This investigation has provided some new insights concerning the mechanisms responsible for storage luminescence in these systems. The occurrence of this phenomenon in the bulk system can be explained by the conventional defect chemistry model, whereas that in the nc counterpart can be attributed to a different mechanism, viz, exciton mediated process induced by chemisorbed species.

Acknowledgment. Our special thanks go to Dr. G. N. Subbanna for the help in getting TEM pictures, and J.D acknowledges gratefully the CSIR, New Delhi for a Junior Research Fellowship received. Also our sincere thanks to CECRI/CSIR, New Delhi, and NTU/NSC, Taipei for all of the facilities we received in this work.

References and Notes

(1) Shen, Y.; Friend, C. S.; Jiang, Y.; Jakubczyk, D.; Swiatkiewicz, J.; Prasad, P. N. *J. Phys. Chem. B.* **2000**, *104*, *7577*.
(2) Chang, W.; Cosandey, F.; Hahn, H. *Nanostruct. Mater*. 1993, *2*, 29.
(3) Kobayashi, M. *J. Mater. Sci. Lett.* **1992**, *11*, 767.
(4) Sekar, M. M. A.; Manoharan, S. S.; Patil, K. C. *J. Mater. Sci. Lett.* **1990**, *9*, 1205.
(5) Hase, T.; Kano, T.; Nakazawa, E.; Yamamoto, H. *Adv. Electron. Phys.* **1990**, *79*, 271.
(6) Justel, T.; Bechtel, H.; Nikol, H.; Ronda, C. R.; Wiechert, D. U. *Proc. VII Int. Symp. Luminescent Mater. Electrochem. Soc. Proc.* **1998**, *98*−*24*, 103.
(7) Eychmuller, A. *J. Phys. Chem. B.* **2000**, *104*, 6514.
(8) Varma, H. K.; Mukundan, P.; Warrier, K. G. K.; Damodaran, A. D. *J. Mater. Sci. Lett.* **1990**, *9*, 377.
(9) Pramanik, P. *Bull. Mater. Sci.* **1995**, *18*, 819.
(10) Sin, A.; Odier, P. *Adv. Mater.* **2000**, *12*, 649.
(11) Konnrad, A.; Fries, T.; Gahn, A.; Kummer, F.; Herr, U.; Tidecks, R.; Samwer, K. *J. Appl. Phys.* **1999**, *86*, 3129.
(12) Williams, D. K.; Eilers, H.; Tissue, B. M.; McHale, J. M. *J. Phys. Chem. B* **1998**, *102*, 916.
(13) Eilers, H.; Tissue, B. M. *Chem. Phys. Lett.* **1996**, *251*, 74.
(14) Bihari, B.; Eilers, H.; Tissue, B. M. *J. Lumin.* **1997**, *75*, 1.
(15) Jagannathan, R.; Kutty, T. R. N.; Kottaisamy, M.; Jeyagopal, P. *Jpn. J. Appl. Phys.* **1994**, *33*, 6207.
(16) Jagannathan, R.; Watanabe, M.; Murase, N.; Karthikeyani, A.; Kanematsu, Y.; Kitamura, N.; Yazawa, T.; Kushida, T. *J. Appl. Phys.* **1998**, *83*, 911.
(17) Klug, H. P.; Alexander, L. E. *X-ray Diffraction Procedures for Polycrystalline and Amorphous Materials*, 2nd ed.; Wiley-Interscience: NewYork, 1974.
(18) Adam, J. L.; Poncon, V.; Lucas, J.; Boulon, G. *J. Non-Cryst. Solids* **1987**, *91*, 191.
(19) Blasse, G.; Grabmaier, B. C. *Luminescent Materials*; Springer: Berlin, Germany, 1994.
(20) Tomiki, T.; Tamashiro, J.; Tanahara, Y.; Yamada, A.; Fukutani, H.; Miyahara, T.; Yamada, A.; Fukutani, H.; Miyahara, T.; Kato, H.; Shin, S.; Ishigame, M. *J. Phys. Soc. Jpn.* **1986**, *55*, 4543.
(21) Jollet, F.; Noguera, C.; Thromat, N.; Gautier, M.; Duraud, J. P. *Phys. Rev. B* **1990**, *42*, 7587.
(22) Schmechel, R.; Kennedy, M.; von Seggern, H; Winkler, H.; Kolbe, M.; Fischer, R. A.; Xaomao, Li.; Benker, A.; Winterer, M.; Hahn, H. *J. Appl. Phys.* **2001**, *89*, 1679.
(23) Van Schaik, W.; Blasse, G. *Chem. Mater.* **1992**, *4*, 410.
(24) Ronda, C. R. *J. Lumin.* **1997**, *72*, *49*.
(25) Barnes, M. D.; Mehta, A.; Thundat, T.; Bhargava, R. N.; Chhabra, V.; Kulkarni, B. *J. Phys. Chem. B* **2000**, *104*, 6099.
(26) Nirmal, M.; Dabbousi, B. O.; Bawendi, M. G.; Macklin, J. J.; Trautman, J. K.; Harries, T. D.; Brus, L. E. *Nature* 1996, *383*, 802.